NASA CONTRACTOR REPORT

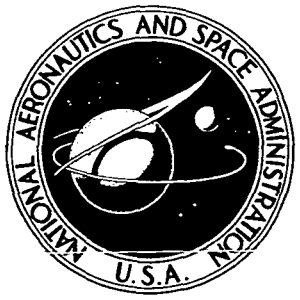

NASA CR-2491

NASA CR-2491

SKIN FRICTION REDUCTION IN SUPERSONIC FLOW BY INJECTION THROUGH SLOTS, POROUS SECTIONS AND COMBINATIONS OF THE TWO

Joseph A. Schetz and Johannes vanOvereem

Prepared by
VIRGINIA POLYTECHNIC INSTITUTE AND STATE UNIVERSITY
Blacksburg, Va. 24060
for Langley Research Center

NATIONAL AERONAUTICS AND SPACE ADMINISTRATION • WASHINGTON, D. C. • MARCH 1975

1. Report No.	2. Government Accession No.	3. Recipient's Catalog No.
NASA CR-2491		

4. Title and Subtitle	5. Report Date
SKIN FRICTION REDUCTION IN SUPERSONIC FLOW BY INJECTION THROUGH SLOTS, POROUS SECTIONS AND COMBINATIONS OF THE TWO	MARCH 1975
	6. Performing Organization Code

7. Author(s)	8. Performing Organization Report No.
Joseph A. Schetz and Johannes vanOvereem	
	10. Work Unit No.

9. Performing Organization Name and Address	11. Contract or Grant No.
Aerospace and Ocean Engineering Department Virginia Polytechnic Institute and State University Blacksburg, Virginia 24060	NGR-47-004-160
	13. Type of Report and Period Covered

12. Sponsoring Agency Name and Address	13. Type of Report and Period Covered
National Aeronautics and Space Administration Washington, D.C. 20546	Contractor Report
	14. Sponsoring Agency Code

15. Supplementary Notes

Final Report

16. Abstract An experimental study of skin friction reduction in a Mach 3.0 air steam with gaseous injection through a tangential slot, a porous wall section and combinations of the two was conducted. The primary data obtained were wall shear values measured directly with a floating element balance and also inferred from Preston Tube measurements. Detailed profiles at several axial stations, wall pressure distributions and Schlieren photographs are presented. The data indicate that a slot provides the greatest skin friction reduction in comparison with a reference flat plate experiment. The porous wall section arrangement suffers from an apparent roughness-induced rise in skin friction at low injection rates compared to the flat plate. The combination schemes demonstrated a potential for gain.

17. Key Words (Suggested by Author(s))	18. Distribution Statement
slot injection experiment porous wall injection supersonic turbulent boundary layer skin friction balance data	Unclassified - Unlimited Subject Category 34 Fluid Mechanics and Heat Transfer

19. Security Classif. (of this report)	20. Security Classif. (of this page)	21. No. of Pages	22. Price*
Unclassified	Unclassified	61	$4.25

*For sale by the National Technical Information Service, Springfield, Virginia 22151

TABLE OF CONTENTS

TABLE OF CONTENTS(cont'd.)

LIST OF SYMBOLS

a	Slot height
D	Diameter
$\dot{m}_j$	Mass flow rate of injectant
M	Mach number
p	Pressure
p_o	Stagnation pressure
p'_o	Pitot pressure
p_c	Cone pressure
U	Streamwise Velocity
x	Streamwise distance measured from the slot exit station
y	Normal distance
τ_w	Wall shear
ρ	Density

Subscripts

∞	Free stream conditions ahead of injection
e	Edge conditions
j	Slot conditions
w	Wall conditions
t	Reservoir conditions for main flow

SKIN FRICTION REDUCTION IN SUPERSONIC FLOW BY INJECTION THROUGH SLOTS, POROUS SECTIONS AND COMBINATIONS OF THE TWO

By Joseph A. Schetz and Johannes vanOvereem
Virginia Polytechnic Institute and State University

INTRODUCTION

Fluid injection schemes for thermal protection and, more recently, skin friction reduction on flight vehicles have been the subject of study for some time. Energy conservation considerations have now elevated the importance of the skin friction reduction application. The experimental information available at supersonic speeds (e.g. Refs. (1) - (3)) is limited but sufficient to indicate that drag reductions large enough to be interesting from an overall systems viewpoint may be achievable. The main, competing configurations are the porous wall, and the tangential slot. There have been few studies where a direct comparison of the two schemes was made at the same nominal conditions and where the flow field was completely documented. Further, combinations of the two schemes might be expected to be beneficial as a result of synergistic interactions. Strong motivation for studying combinations of slot and porous wall injection may be derived from overall systems studies that indicate that a mucn more rapid decrease in skin friction as a function of injectant mass flow rate than has been achieved for porous wall injection alone will be required for successful paractical application.

This report presents the results of a comparative study of slot injection, porous wall injection through a short strip of surface and combinations of the two at free stream conditions of Mach 2.9, stagnation pressure of 6.9 N/m^2 (150 psia) and total temperature of 290°K. A "flat plate", solid wall configuration was also studied as a reference point. Total injectant rates covering a wide range were considered. The principal data obtained were:

(1) schlieren photographs, (2) wall pressure distributions, (3) Mach Number profiles at four axial stations and (4) wall shear measured with a self-nulling, floating element balance. Wall shear data was also inferred from Preston Tube measurements.

In the next section, the experimental apparatus, including the wind tunnel, the model, the probes, the skin friction balance, the instrumentation, and the optical equipment is described in detail. The succeeding sections outline the test procedure, data reduction and experimental results. An error analysis is given in Appendix A.

EXPERIMENTAL APPARATUS

A. WIND TUNNEL

These experiments were performed in the 23 cm x 23 cm supersonic wind tunnel at VPI&SU. This tunnel was designed and originally constructed at the Langley Aeronautical Laboratory. The facility is of an intermittent, blow-down type with interchangeable contoured nozzles. However, for this work a special nozzle arrangement was constructed to incorporate the model into the nozzle. The air is pumped by eight Ingersoll Rand, Model 90, reciprocating compressors and stored in sixteen storage tanks with a total volume 79.3 cubic meters. At present, the maximum pressure obtainable by the compressors is 10.4 N/m^2 (150 psia) in these tanks. The tunnel is activated by a quick opening butterfly valve with a variable speed control.

The settling chamber contains a perforated transition cone, several dampening screens, and probes to measure stagnation pressure and temperature. After passing through the test section and diffuser, the air is dumped into the atmosphere.

B. THE MODEL

The model was a modified version of the interchangeable contoured nozzles generally used in this wind tunnel. The streamline normally produced at the axis of a two-dimensional, symmetric supersonic nozzle is replaced by a solid surface. Just beyond the last expansion wave in the nozzle, the surface steps down (0.64 cm) to form the slot for the slot injection cases (See Fig. 1(a)). The slot lip is 0.041 cm. thick. This special

nozzle configuration allows ample room for a plenum chamber for the injected gas and uniformly distributes and straightens the slot flow thereby insuring a uniform, two-dimensional injected flow. The block for the upper half of the nozzle was selected to give a Mach number of approximately 3.0. The bottom of the model was then designed in several sections. The first two are of little importance except that they were designed to be compatible with the upper half. Also the second section, which was designated the dummy section, had three stations so that a spanwise survey of static pressure could be made upstream of the injection station to ascertain the two dimensionality of the experiment.

The injection "boxes" were designed such that a uniform two-dimensional flow could be obtained from a pipe which is essentially a point source. In order to achieve these desired results, the air flow was supplied to the bottom of these sections through a header which was fabricated from a pipe with holes drilled in such a manner as to provide more escape area toward the ends of the header since the air entered in the middle. For the slot box, the flow then passes through a flow straightener (5 cm long) in the flow direction. This was constructed by placing about four hundred plastic straws between wire screens. This arrangement gave a very uniform flow as shown by the spanwise static pressure distributions.

The porous injection box measures 5.08 cm. in the streamwise direction and spans the tunnel. There is a solid section 0.64 cm. long at the upstream and downstream edges; the middle 3.81 cm. length is porous, sintered stainless steel (65 micron mean porosity), 0.64 cm. thick. For porous-wall tests, the box was arranged as in Fig. 1(b), and no injectant was fed through the slot box. For the combined slot/porous wall tests, the two boxes were arranged as in Fig. 1(c).

The final section of the nozzle was a wall made of polished 304 stainless steel which was instrumented with static pressure taps and thermocouples in both the streamwise and spanwise directions. The static pressure taps were 0.787 mm in diameter and the thermocouples were 0.25 mm copper-constantan wire press fitted on the plate's surface. The instrumentation locations and their relative position to the slot is shown in Figure 2. Also shown in this figure are the locations of the four stations where the vertical

measurements were taken. This instrumented plate was followed by a ramp in order to bring the flow into the diffuser.

A "flat plate" configuration was obtained by raising the instrumented section upward 0.64 cm. from that shown in Fig. 1(a), hence a solid, flat surface was aligned with the free stream flow.

Photographs of the model for the three test configurations are given in Fig. 3.

INSTRUMENTATION

A. SKIN FRICTION BALANCE

The skin friction balance used in these experiments is described in detail in Ref. (4). Essentially, the balance is designed as a null-type device in that the deflections of the floating head element due to shear are returned to zero by a servodrive mechanism. The balance was designed to operate in a horizontal position, however in these experiments the unit was used in an upright mode. In the former position gravity was used to supply a small amount of tension to the servomechanism. Here, the problem was solved with a small spring opposed to the spring connecting the balance arm and servodrive. Also of note, is the fact that the balance did not incorporate the cooling mechanism described in Ref. (4). The linear variable differential transformer (LVDT) is excited by a carrier amplifier which is in turn amplified by an amplifier which drives the servomotor. The servomotor returns the LVDT to zero and at the same time activates a potentiometer whose output is recorded on the strip recorders indicating the shear load. To relate the output on the recorders to the shear loads incurred, a calibration arm was added on the balance arm.

The floating head of the balance was made oblong in the lateral or spanwise direction to minimize the pressure gradient effects. The area of the floating element was 3.200 cm^2, and the surface of the test section wall and floating head were flush to within ± 0.0025 cm for all tests.

Both the floating head and the upper lever arm of the balance were made of aluminum to allow careful mechanical balancing of the entire system.

B. PRESSURE PROBES

Three sets of probes were used to measure pressures in the flow. These pressures are used to deduce Mach number number distributions and surface shear via the Preston Tube technique.

All pressures were read using strain gauge transducers which were calibrated within ±.15% of their individual full scale ranges. Transducer outputs were read on Hewlett-Packard strip chart recorders with a microvolt sensitivity ±.1% full scale.

The wall pressures, the cone-static pressure probe, and the pitot rake, described below, were read using a model 48J9-1021 Scani-valve.

Cone Static probes.-- The cone static probe used a 10^{o} ± 2' semivertex angle brass cone with base diameter of 0.157 cm soldered to 0.160 cm stainless steel tubing. The tip was precision ground and extreme care had to be exercised to keep the vertex at its assigned value. Four 0.033 cm ports were drilled perpendicular to the cone's surface approximately three quarters back from the tip at 90^{o} intervals around the circumference. The four ports were connected to a common chamber, thus the recorded pressures were the average pressures and angle of attack effects were reduced to a minimum.

Pitot probes.-- Two types of pitot probes were used out in the flow. One was used in conjunction with the cone-static probe at the outer edge of the boundary layer to obtain the local free-stream static pressure and hence Mach number. The probe tip was made by flattening 0.318 cm O.D. stainless steel circular tubing to a rectangular cross section. The opening on each probe was 0.0254 cm high with a lip thickness of approximately 0.0203 cm. The second type of pitot probe was simply 0.071 cm. O.D., 0.041 cm. I.D. stainless steel tubes mounted on a thin rake. The rake consisted of 12 probes, equally spaced at intervals of 0.127 cm. up from the wall.

Preston Tubes.--Two sizes of Preston tubes (0.073 and 0.241 cm. O.D. both with I.D./O.D. = 0.6) were used. They were chosen to correspond to cases near the minimum and maximum size suggested in Ref. (5) based upon the "flat plate" boundary layer.

C. OPTICS

For schlieren pictures, a continuous collimated beam of light was passed

through the test section using the PEK model 910 L.H. light source and PEK type 107 lens. The mirrors were 30.5 cm. diam. and had a focal length of 2.03 m. Exposures times were one millisecond. All photographs were taken on Polaroid type 57 (ASA 3000) sheet film using a Graflex camera. The windows of the test section were ground and polished to ± 15 arc seconds which is of schlieren quality.

D. FLOW METERS

The flow rates of the various injectant streams were determined with ASME Orifice plate flow meters placed in each supply line. These meters were constructed, installed and operated in accordance with Ref. (6).

DATA REDUCTION

The directly measured wall shear force data were obtained from the balance readings and calibration curves. The wall pressure distributions were obtained via transducer calibrations.

The Mach number profiles were determined by processing the edge cone-static and pitot probe and the pitot rake data as follows. First, the cone pressure and pitot pressure were used to find the edge Mach number as

$$\frac{p_c}{p_o'} = \left[\frac{p_c}{p}\right]\left[\frac{p}{p_o}\right]\left[\frac{p_o}{p_o'}\right]$$

all of which are functions of Mach number only. A plot of p_c/p_o' versus M was then made. The quantity p_c/p was obtained from Ref. (7), and Ref. (8) was used for the remaining two ratios. Using the calculated M and measured p_o', p_o and p were determined. It was then assumed that the static pressure was constant across the shear layer (previous work in Ref. (3) had indicated that this was a good approximation), and this static pressure was combined with the pitot pressures on the rake to obtain corresponding Mach number values.

The Preston Tube data was processed as suggested in Ref. (5) with the static pressure obtained as above.

RESULTS

A. FLOW VISUALIZATION

A Schlieren photograph was taken for every test run to insure that the tunnel was operating properly and that the probes were intact. Typical examples are shown in Figs. 4(a),(b),(c) where the main flow is from left to right. Pictures of this type are extremely helpful in understanding the qualitative aspects of the flow field and in interpreting the detailed profile measurements. It can be noted that the initial boundary layer thickness at the injection station is somewhat greater than the slot height. The boundary layer is also turbulent.

For the porous wall injection case in Fig. 4(b), weak shock waves are produced at the joints between the injection box and the other sections and between the solid and porous surfaces of the box itself. The thickening of the boundary layer as a result of the normal injection is apparent.

For the over-expanded slot injection case shown in Fig. 4(a), one can clearly see the adjustment required at the injection station in order to match the static pressure on each side of the dividing streamline emanating from the slot lip. The higher pressure free stream turns through an expansion fan toward the wall, and the injectant stream is compressed. After a length equal to several slot heights, the free stream turns back parallel to the model surface through a distributed recompression region. A lip shock produced by viscous interactions near the lip of the finite thickness splitter plate is visible. It is interesting to observe the curvature in this weak shock as it proceeds out from the lip through the vortical flow of the splitter plate boundary layer. An additional, perhaps important, feature of the flow is the wake produced by the slot lip which can be discerned as a dark band through the middle of the mixing region. This appears to extend as a separate identifiable region for a downstream distance of several slot heights.

The combined slot/porous wall injection case in Fig. 4(c) displays a combination of the features of the slot and the porous wall injection. The most interesting features are the thickening of the wall boundary layer and the reduced turning of the shear layer.

B. PROFILE MEASUREMENTS

The cone-static and pitot pressure measurements were processed to give

distributions of Mach number across the mixing region. Profiles are presented in Fig. 5(a),(b) and (c). The data are also tabulated in Appendix B. The viscous mixing region is clearly delineated and the effects of the free stream adjustments can be seen at the outer edge of the profiles. The combined effects of viscous forces, axial pressure gradients and gross turning of the flow to make the necessary initial pressure adjustments are displayed here in detail. Finally, with the plausible assumption of constant total temperature, these profiles can be easily converted into velocity profiles.

C. WALL PRESSURE DISTRIBUTIONS

Wall pressure distributions were measured for all cases studied. The data corresponding to the locations were the profiles were obtained are given in Fig. 6(a), (b) and (c). The recompression region for the underexpanded slot injection cases is apparent. Finally, no wall pressure data were obtained in the porous wall regions themselves for any of the cases. The tabulated data are presented in Appendix C.

D. WALL SHEAR MEASUREMENTS

Wall shear data were obtained directly with the floating element balance and indirectly via Preston Tube measurements. The balance data is presented with the Preston Tube data then used for comparison with the balance data. All the data were taken at an axial distance of 12.7 cm from the end of the slot (X/a = 20). This corresponds to station "b" in Fig. 1(a) and station "a" in Figs. 1(b) and 1(c).

Floating Element Balance Data.-- The presentation of the slot/porous wall combination data required the choice of a new coordinate system, since the conventional choices were no longer suitable or informative. Indeed, it was decided to present the data for the two separate configurations on this new type of plot also for purposes of direct comparison. In Fig. 7, the horizontal axis of the graph has been selected to reflect the actual total mass flow injected, non-dimensionalized by the mass flow through a unit area of the free stream. This has been done so that systems decisions for a practical scheme are more easily reached. The vertical axis is simply a skin friction coefficient based upon edge conditions ahead of injection.

A very sharp reduction in wall shear is clearly produced with increasing

injection rate down to a minimum in each case. Clearly, the tangential slot provides the greatest reduction in wall shear per unit rate of injection. Helium proved to be a more effective injectant than air for the slot configuration.

The porous wall schemes apparently suffer from a roughness-induced initial rise in shear at low injection rates. Further study will be required with the "roughness" of practical porous sections correctly scaled to the flight sublayer thickness before final conclusions can be drawn. There does seem to be a potential for gain by combining slot and porous injection if the roughness-induced initial rise can be reduced. This assessment is based upon a consideration of the points labelled "a, c and d" clustered in the middle of Fig. 7. Point "a" corresponds to the slot/porous wall configuration (Fig. 1(c)) but with all the injection through the slot. The resulting skin friction is higher than that for the slot-only configuration at the same injection rate as a result of the roughness of the porous wall insert. Point "d" corresponds to the same injection rate but with 50% through the porous wall section. The skin friction is reduced. Thus, if the roughness induced rise in skin friction could be eliminated or minimized, the combination scheme might produce results below the slot-only results. The data are tabulated in Appendix D.

Preston Tube Data.--In order to avoid greater confusion on the plots, the Preston Tube results are presented separately for the slot-only and porous-wall-only cases in Figs. 8(a) and (b). Also included for comparison is a fairing of the balance data from above. Some comments are in order. First, the Preston Tube is clearly capable of providing very useful information for mass injection flows. This is especially true if one were to recast the results as C_f/C_{f_o}, since the shape of the curves is very well predicted. Second, the larger Preston Tube consistently gave the best quantitative results. This is presumably a result of the fact that the smaller tube was near the minimum suggested based upon the "flat plate" boundary layer size. With injection, the viscous region was generally sharply increased in thickness. Also, the data in Ref. (5) showed the best results with tubes nearer the maximum size. The tabulated data is given in Appendix E.

CONCLUDING REMARKS

The experimental results obtained here suggest several conclusions. First, systems employing porous walls appear to suffer from a roughness-induced increase in wall shear at low injection rates. Clearly, more detailed study of this phenomena is warranted. Second, the tangential slot arrangement provides the greatest reduction in wall shear per unit mass of injectant. Third, for slot injection, helium was more effective per unit mass of injection than air. Fourth, the present limited results indicate a potential for gain in the combined slot/porous-wall arrangement. Last, the Preston Tube is capable of quite acceptable measurements of skin friction for the types of flows studied here.

REFERENCES

1. McRee, D. I., Peterson, J. B. and Braslow, A. L., "Effect of Air Injection Through a Porous Surface and Through Slots on Turbulent Skin Friction at Mach 3," NASA TN D-2427, Aug. 1964.
2. Cary, A. M. and Hefner, J. N., "An Investigation of Film Cooling Effectiveness and Skin Friction in Hypersonic Turbulent Flow", AIAA Paper No. 70, June 1971.
3. Kenworthy, M. and Schetz, J. A., "An Experimental Study of Slot Injection into a Supersonic Stream," AIAA Journal, Vol. 11, No. 5, May 1973.
4. Bruno, J. R., Yanta, W. J., and Richer, D. B., "Balance for Measuring Skin Friction in the Presence of Heat Transfer", NOLTR 69-56, 10 June 1969.
5. Allen, J. M., "Evaluation of Compressible Flow Preston Tube Calibrations," NASA TN D-7190, May 1973.
6. ASME Power Test Codes, Pt. 5, Ch. 4, "Flow Measurements", ASME, New York, 1959.
7. Sims, J. L., Tables for Supersonic Flow Around Right Circular Cones at Zero Angle of Attack, NASA SP-3004, 1964.
8. Equations, Tables, and Charts for Compressible Flow, NACA 1135, 1953.
9. Waltrup, P. J. and Schetz, J. A., "An Experimental Investigation of a Compressible Boundary Layer Subjected to a Systematic Variation of Adverse Pressure Gradients", VPI-E-71-18, August 1971.
10. O'Donnell, F. B. and Westkaemper, J. C., "Measurements of Errors caused by Misalignment of Floating-Element Skin-Friction Balances", AIAA Journal, Vol. 3, Number 1, January 1965.

APPENDIX A: ERROR ANALYSIS

In this section, we present estimates of the maximum experimental errors involved in the various measurements. The basic measurements made in the flow were pitot and cone static pressures from which the Mach profiles were derived, therefore let us start the analysis here.

Pitot Pressures.-- The errors incurred here were the sum of: 1) reading from the strip chart recorders; 2) turbulence in the shear layer; 3) calibration; and 4) response time. All of these are small and in some instances do not apply, for example the reservoir pitot pressure had no response error. As was estimated in detail in Ref. (10) for similar flow conditions, these measurements were within $\pm$ 0.5% of the true value.

Cone Static.-- Errors incurred making these measurements were estimated to be slightly less than those incurred for the pitot pressures. This is due to the fact that the gradients encountered were much less and the turbulence level had little effect on the static pressure. However, in order to make a conservative estimate of all errors, the error here will be set at $\pm$ 0.5%.

Pressure Ratios.-- The reservoir pressure was constant during any run to within a maximum of about $\pm$ 1.5%, thus the ratios, without consideration of position, would be $\pm$ 3.0% of their actual values.

Mach Number Profiles.-- Since the pressure ratios used to determine the Mach profiles are within $\pm$ 3.0% let us examine the pressure ratio $p_c/p_o' = 0.1860$ which gives a typical Mach number of 2.40.

$$(+3.0\%)\ \frac{p_c}{p_o'} = 0.1916 \qquad M = 2.35\ (-2\%)$$

$$(-3.0\%)\ \frac{p_c}{p_o'} = 0.1804 \qquad M = 2.45\ (2\%)$$

Hence an error in the pressure ratios of $\pm$ 3.0% yields Mach number within $\pm$ 2%.

Skin Friction.-- For the skin friction balance, the estimates of Ref. (9) may be assumed to apply here which indicate that the error due to the skin friction balance are $\pm$ 6% due to tunnel noise, amplifiers, and recorders. Also, from Ref. (10), an additional error of $\pm$ 1% due to misalignment of the floating element should be added yielding an error of $\pm$ 7%. For the Preston Tube data, the results of Ref. (5) indicate an error of 10% is to be expected.

APPENDIX B

Tabulated Profile Data

TABLE B-1

"Initial" Profile Upstream of the Slot Exit Station

x = 0.0 cm.

$p_{c,e} = 3.686 \frac{N}{cm^2}$, $p'_{o,e} = 25.000 \frac{N}{cm^2}$, $M_e = 2.72$, $p_e = 3.573 \frac{N}{cm^2}$

Probe No.	Y, cm	p'_o, N/cm^2	M
1	0.127	10.569	1.700
2	0.254	14.459	2.030
3	0.381	18.866	2.343
4	0.508	21.314	2.500
5	0.635	24.741	2.705
6	0.762	25.189	2.730
7	0.889	25.259	2.735
8	1.016	25.070	2.720
9	1.143	24.811	2.710
10	1.270	25.140	2.730
11	1.397	25.161	2.730
12	1.524	25.000	2.720

Slot only (rake at slot):

(1) $M_j = 0.55$ at $\dot{m}_j = 52.6$ gm/sec

(2) $M_j = 0.53$ at $\dot{m}_j = 42.7$ gm/sec

(3) $M_j = 0.58$ at $\dot{m}_j = 29.5$ gm/sec

TABLE B-2

Profiles for Slot Injection Cases

$$\frac{\dot{m}_j}{\rho_\infty u_\infty (1)} = 6.94 \times 10^{-4}$$

$$x = 2.54 \text{ cm.}$$

$$p_{c,e} = 3.204 \frac{N}{cm^2}, \quad p'_{o,e} = 23.181 \frac{N}{cm^2}, \quad M_e - 2.85, \quad p_e = 2.120 \frac{N}{cm^2}$$

Probe No.	Y	p'_o	M
	cm	N/cm^2	
1	0.127	2.574	0.534
2	0.254	2.455	0.463
3	0.381	2.784	0.636
4	0.508	4.064	1.011
5	0.635	8.261	1.623
6	0.762	12.570	2.0555
7	0.889	16.417	2.375
8	1.016	19.873	2.629
9	1.143	22.643	2.815
10	1.270	22.972	2.837
11	1.397	23.090	2.844
12	1.524	23.181	2.850

TABLE B-2

Profiles for Slot Injection Cases

$$\frac{\dot{m}_j}{\rho_\infty u_\infty (1)} = 7.36 \times 10^{-4}$$

$x = 7.62$ cm.

$p_{c,e} = 3.253 \ \frac{N}{cm^2}$, $p'_{o,e} = 23.461 \ \frac{N}{cm^2}$ $M_e = 2.85$, $p_e = 2.146 \ \frac{N}{cm^2}$

Probe No.	Y cm	p'_o N/cm^2	M
1	0.127	3.015	0.714
2	0.254	3.414	0.842
3	0.381	5.001	1.172
4	0.508	7.911	1.570
5	0.635	12.549	2.040
6	0.762	17.117	2.413
7	0.889	21.202	2.703
8	1.016	23.580	2.858
9	1.143	24.112	2.891
10	1.270	23.951	2.881
11	1.397	23.650	2.862
12	1.524	23.461	2.850

TABLE B-2

Profiles for Slot Injection Cases

$$\frac{\dot{m}_j}{\rho_\infty u_\infty (1)} = 7.26 \times 10^{-4}$$

$$x = 12.7 \text{ cm.}$$

$$p_{c,e} = 3.388 \frac{N}{cm^2}, \quad p'_{o,e} = 24.466 \frac{N}{cm^2}, \quad M_e = 2.85, \quad p_e = 2.238 \frac{N}{cm^2}$$

Probe No.	Y	p'_o	M
	cm	N/cm^2	
1	0.127	4.414	1.035
2	0.254	5.393	1.201
3	0.381	7.583	1.493
4	0.508	10.730	1.828
5	0.635	14.906	2.190
6	0.762	19.355	2.519
7	0.889	22.923	2.755
8	1.016	24.420	2.847
9	1.143	24.559	2.856
10	1.270	24.462	2.850
11	1.397	24.371	2.844
12	1.524	24.462	2.850

TABLE B-3

Profiles for Porous Wall Injection Cases

$$\frac{\dot{m}_j}{\rho_\infty u_\infty \ (1)} = 1.072 \times 10^{-3}$$

$$x = 7.62 \text{ cm.}$$

$$p_{c,e} = 3.707 \frac{N}{cm^2}, \quad p'_{o,e} = 26.392 \frac{N}{cm^2}, \quad M_e = 2.82, \quad p_e = 2.463 \frac{N}{cm^2}$$

Probe No.	Y cm	p'_o N/cm^2	M
1	0.127	5.923	1.200
2	0.254	8.604	1.520
3	0.381	12.682	1.900
4	0.508	16.928	2.230
5	0.635	21.125	2.510
6	0.762	24.084	2.690
7	0.889	25.014	2.740
8	1.016	25.063	2.740
9	1.143	25.084	2.750
10	1.270	24.972	2.740
11	1.397	24.573	2.720
12	1.524	26.392	2.820

TABLE B-3

Profiles for Porous Wall Injection Cases

$$\frac{\dot{m}_j}{\rho_\infty u_\infty (1)} = 1.034 \times 10^{-3}$$

$$x = 12.7 \text{ cm.}$$

$$p_{c,e} = 3.567 \frac{N}{cm^2}, \quad p'_{o,e} = 24.343 \frac{N}{cm^2}, \quad M_e = 2.73, \quad p_e = 2.417 \frac{N}{cm^2}$$

Probe No.	Y	p'_o	M
	cm	N/cm^2	
1	0.127	7.079	1.365
2	0.254	9.070	1.590
3	0.381	12.213	1.880
4	0.508	15.949	2.180
5	0.635	19.726	2.443
6	0.762	23.223	2.663
7	0.889	24.224	2.723
8	1.016	24.273	2.726
9	1.143	24.315	2.728
10	1.270	24.385	2.733
11	1.397	24.294	2.727
12	1.524	24.105	2.715

TABLE B-3

Profiles for Porous Wall Injection Cases

$$\frac{\dot{m}_j}{\rho_\infty u_\infty (1)} = 5.76 \times 10^{-4}$$

$$x = 7.62 \text{ cm.}$$

$$p_{c,e} = 3.630 \frac{N}{cm^2}, \quad p'_{o,e} = 25.616 \frac{N}{cm^2}, \quad M_e = 2.80, \quad \bar{p}_e = 2.423 \frac{N}{cm^2}$$

Probe No.	Y	p'_o	M
	cm	N/cm^2	
1	0.127	5.260	1.114
2	0.254	7.431	1.405
3	0.381	10.998	1.770
4	0.508	14.822	2.090
5	0.635	19.042	2.390
6	0.762	22.559	2.650
7	0.889	24.615	2.740
8	1.016	24.706	2.750
9	1.143	24.706	2.750
10	1.270	24.056	2.710
11	1.397	24.196	2.720
12	1.524	-	-

TABLE B-3

Profiles for Porous Wall Injection Cases

$$\frac{\dot{m}_j}{\rho_\infty u_\infty (1)} = 5.51 \times 10^{-4}$$

$$x = 17.78 \text{ cm.}$$

$$p_{c,e} = 3.477 \frac{N}{cm^2}, \quad p'_{o,e} = 24.762 \frac{N}{cm^2}, \quad M_e = 2.82, \quad p_e = 2.311 \frac{N}{cm^2}$$

Probe No.	Y cm	p'_o N/cm^2	M
1	0.127	7.324	1.430
2	0.254	8.954	1.620
3	0.381	11.262	1.844
4	0.508	14.081	2.087
5	0.635	17.816	2.387
6	0.762	21.496	2.620
7	0.889	24.084	2.780
8	1.016	24.811	2.820
9	1.143	24.811	2.820
10	1.270	24.783	2.820
11	1.397	24.832	2.820
12	1.524	24.762	2.820

TABLE B-4

Profiles for Slot/Porous Wall Injection Cases

$$\frac{\dot{m}_j}{\rho_\infty u_\infty (1)} = 1.324 \times 10^{-3}$$

$x = 7.62$ cm.

70% Slot/30% Porous

$p_{c,e} = 3.365 \frac{N}{cm^2}$, $p'_{o,e} = 24.112 \frac{N}{cm^2}$, $M_e = 2.84$, $p_e = 2.220 \frac{N}{cm^2}$

Probe No.	Y cm	p'_o N/cm^2	M
1	0.127	2.665	0.512
2	0.254	2.784	0.580
3	0.381	3.365	0.794
4	0.508	4.553	1.067
5	0.635	6.820	1.407
6	0.762	10.402	1.804
7	0.889	15.088	2.215
8	1.016	19.264	2.523
9	1.143	22.741	2.754
10	1.270	24.420	2.860
11	1.397	24.580	2.870
12	1.524	24.112	2.840

TABLE B-4

Profiles for Slot/Porous Wall Injection Cases

$$\frac{\dot{m}_j}{\rho_\infty u_\infty (1)} = 1.324 \times 10^{-3}$$

x = 12.70 cm.

70% Slot/30% Porous

$p_{c,e} = 3.365 \frac{N}{cm^2}$, $p'_{o,e} = 24.161 \frac{N}{cm^2}$, $M_e = 2.84$, $p_e = 2.225 \frac{N}{cm^2}$

Probe No.	Y cm	p'_o N/cm^2	M
1	0.127	3.365	0.792
2	0.254	3.826	0.915
3	0.381	4.876	1.122
4	0.508	6.792	1.400
5	0.635	9.870	1.750
6	0.762	13.857	2.110
7	0.889	18.334	2.455
8	1.016	22.181	2.715
9	1.143	24.070	2.834
10	1.270	24.350	2.851
11	1.397	24.210	2.843
12	1.524	24.161	2.840

TABLE B-4

Profiles for Slot/Porous Wall Injection Cases

$$\frac{\dot{m}_j}{\rho_\infty u_\infty(1)} = 1.324 \times 10^{-3}$$

$x = 17.78$ cm.

70% Slot/30% Porous

$p_{c,e} = 3.365 \frac{N}{cm^2}$, $p'_{o,e} = 24.489 \frac{N}{cm^2}$ $M_e = 2.87$, $p_e = 2.210 \frac{N}{cm^2}$

Probe No.	Y cm	p'_o N/cm^2	M
1	0.127	4.456	1.053
2	0.254	5.225	1.185
3	0.381	6.624	1.376
4	0.508	8.373	1.596
5	0.635	10.940	1.860
6	0.762	14.228	2.150
7	0.889	18.236	2.457
8	1.016	22.083	2.717
9	1.143	24.231	2.854
10	1.270	24.350	2.861
11	1.397	24.231	2.854
12	1.524	24.489	2.870

TABLE B-4

Profiles for Slot/Porous Wall Injection Cases

$$\frac{\dot{m}_j}{\rho_\infty u_\infty (1)} = 1.324 \times 10^{-3}$$

$x = 7.62$ cm.

47.1% Slot/52.9% Porous

$p_{c,e} = 3.295 \frac{N}{cm^2}$, $p'_{o,e} = 23.461 \frac{N}{cm^2}$, $M_e = 2.82$, $p_e = 2.190 \frac{N}{cm^2}$

Probe No.	Y	p'_o	M
	cm	N/cm^2	
1	0.127	2.616	0.510
2	0.254	2.756	0.583
3	0.381	3.365	0.808
4	0.508	4.810	1.125
5	0.635	6.743	1.408
6	0.762	10.283	1.806
7	0.889	14.836	2.210
8	1.016	18.800	2.510
9	1.143	22.181	2.738
10	1.270	23.673	2.837
11	1.397	22.482	2.758
12	1.524		

TABLE B-4

Profiles for Slot/Porous Wall Injection Cases

$$\frac{\dot{m}_j}{\rho_\infty u_\infty (1)} = 1.324 \times 10^{-3}$$

x = 12.7 cm.

47.1% Slot/52.9% Porous

$p_{c,e} = 3.351 \frac{N}{cm^2}$, $p'_{o,e} = 24.105 \frac{N}{cm^2}$, $M_e = 2.84$, $p_e = 2.220 \frac{N}{cm^2}$

Probe No.	Y	p'_o	M
	cm	N/cm^2	
1	0.127	3.584	0.856
2	0.254	4.050	0.968
3	0.381	5.332	1.200
4	0.508	7.431	1.483
5	0.635	10.751	1.839
6	0.762	14.892	2.200
7	0.889	19.369	2.531
8	1.016	22.748	2.755
9	1.143	24.147	2.843
10	1.270	24.147	2.843
11	1.397	24.147	2.843
12	1.524		

TABLE B-4

Profiles for Slot/Porous Wall Injection Cases

$$\frac{\dot{m}_j}{\rho_\infty u_\infty (1)} = 1.324 \times 10^{-3}$$

$$x = 17.78 \text{ cm.}$$

47.1% Slot/52.9% Porous

$p_{c,e} = 3.421 \frac{N}{cm^2}$, $p'_{o,e} = 21.377 \frac{N}{cm^2}$, $M_e = 2.57$, $p_e = 2.379 \frac{N}{cm^2}$

Probe No.	Y	p'_o	M
	cm	N/cm^2	
1	0.127	4.703	1.037
2	0.254	5.612	1.183
3	0.381	7.009	1.370
4	0.508	8.888	1.583
5	0.635	11.535	1.839
6	0.762	14.983	2.124
7	0.889	19.205	2.428
8	1.016	22.867	2.664
9	1.143	24.429	2.758
10	1.270	24.357	2.754
11	1.397	24.245	2.747
12	1.524		

TABLE C-1

Wall Pressure Distribution for Slot Only Case

$$\frac{\dot{m}_j}{\rho_\infty u_\infty(1)} = 7.26 \times 10^{-4}$$

X, cm	pw/po
2.223	0.0239
3.810	0.0242
5.080	0.0244
6.350	0.0247
7.620	0.0278
8.890	0.0271
10.160	0.0271
11.430	0.0279

TABLE C-2

Wall Pressure Distribution for Slot/Porous

Wall Combination Cases

$$\frac{\dot{m}_j}{\rho_\infty u_\infty (1)} = 1.324 \times 10^{-3}$$

70% Slot/30% Porous

X, cm	pw/po
2.223	0.0255
3.810	0.0267
5.080	0.0267
6.350	0.0275
7.620	0.0283
8.890	0.0286
10.160	0.0288

TABLE C-2

Wall Pressure Distribution for Slot/Porous

Wall Combination Cases

$$\frac{\dot{m}_j}{\rho_\infty u_\infty (1)} = 1.324 \times 10^{-3}$$

47% Slot/53% Porous

X, cm	pw/po
2.223	0.0250
3.810	0.0271
5.080	0.0275
6.350	0.0281
7.620	0.0284
8.890	0.0284

APPENDIX D

Tabulated Wall Shear Data from the Skin Friction Balance

TABLE D-1

Wall Shear Distribution for Slot Injection Cases

$x = 12.7$ cm

$\frac{\dot{m}_j}{\rho_\infty u_\infty (1)}$	$C_f = \frac{\tau}{1/2 \rho_e u_e 2}$
2.626×10^{-4}	
3.512×10^{-4}	6.545×10^{-4}
3.867×10^{-4}	5.968×10^{-4}
4.044×10^{-4}	5.721×10^{-4}
4.304×10^{-4}	5.503×10^{-4}
5.451×10^{-4}	5.418×10^{-4}
8.609×10^{-4}	5.116×10^{-4}
10.715×10^{-4}	4.426×10^{-4}
15.823×10^{-4}	3.934×10^{-4}
14.155×10^{-4}	3.082×10^{-4}
18.804×10^{-4}	3.357×10^{-4}
23.828×10^{-4}	3.054×10^{-4}
0	3.138×10^{-4}
	7.3×10^{-4}

TABLE D-2

Wall Shear Distribution for the Flat Plate With A Porous Wall Section

$x = 12.7$ cm

$\frac{\dot{m}_j}{\rho_\infty u_\infty (1)}$	$C_f = \frac{\tau}{1/2 \rho_e u_e^2}$
7.098×10^{-4}	8.092×10^{-4}
10.632×10^{-4}	7.835×10^{-4}
12.508×10^{-4}	7.100×10^{-4}
16.542×10^{-4}	6.666×10^{-4}
18.251×10^{-4}	6.621×10^{-4}
20.107×10^{-4}	5.869×10^{-4}
26.796×10^{-4}	5.453×10^{-4}
30.640×10^{-4}	5.710×10^{-4}
0	9.05×10^{-4}

TABLE D-3

Wall Shear Distribution for Helium Slot Injection

Cases

x = 12.7 cm

$\frac{\dot{m}_j}{\rho_\infty u_\infty (1)}$	$C_f = \frac{\tau}{1/2 \rho_e u_e^2}$
4.211×10^{-4}	4.89×10^{-4}
3.293×10^{-4}	5.63×10^{-4}
2.981×10^{-4}	6.10×10^{-4}
4.252×10^{-4}	4.723×10^{-4}
3.345×10^{-4}	4.99×10^{-4}

TABLE D-4

Wall Shear Distribution for Slot/Porous

Wall Combination Cases

x = 12.7 cm

% Porous Total Flow	$\frac{\dot{m}_j}{\rho_\infty u_\infty (1)}$	$C_f = \frac{\tau}{1/2\ \rho_e u_e^2}$
33.67	12.518×10^{-4}	4.837×10^{-4}
49.87	12.034×10^{-4}	4.728×10^{-4}
0.00	4.893×10^{-4}	12.28×10^{-4}
16.40	9.245×10^{-4}	6.584×10^{-4}
15.00	7.192×10^{-4}	6.755×10^{-4}
0.00	7.458×10^{-4}	8.487×10^{-4}

APPENDIX E

Tabulated Preston Tube Data

TABLE E-1

Preston Tube Data for Slot Injection Cases

$x = 12.7$ cm

$D = 0.073$ cm

$\frac{\dot{m}_j}{\rho_\infty u_\infty (1)}$	$C_f = \frac{\tau}{1/2 \rho_e u_e 2}$
23.83×10^{-4}	5.10×10^{-4}
23.35×10^{-4}	4.19×10^{-4}
22.41×10^{-4}	5.12×10^{-4}
16.34×10^{-4}	5.10×10^{-4}
16.28×10^{-4}	5.42×10^{-4}
14.38×10^{-4}	5.88×10^{-4}
12.12×10^{-4}	6.46×10^{-4}
7.68×10^{-4}	7.83×10^{-4}
5.10×10^{-4}	8.89×10^{-4}
5.07×10^{-4}	9.04×10^{-4}
4.91×10^{-4}	9.13×10^{-4}
4.41×10^{-4}	9.33×10^{-4}
3.86×10^{-4}	9.53×10^{-4}
3.55×10^{-4}	9.73×10^{-4}
0	13.19×10^{-4}

TABLE E-2

Preston Tube Data for Slot Injection Cases

$x = 12.7$ cm

$D = 0.241$ cm

$\frac{\dot{m}_j}{\rho_\infty u_\infty (1)}$	$C_f = \frac{\tau}{1/2 \rho_e u_e^2}$
0	8.95×10^{-4}
23.83×10^{-4}	4.62×10^{-4}
23.35×10^{-4}	3.22×10^{-4}
22.41×10^{-4}	4.43×10^{-4}
16.34×10^{-4}	4.11×10^{-4}
16.28×10^{-4}	4.03×10^{-4}
14.38×10^{-4}	4.22×10^{-4}
12.12×10^{-4}	4.69×10^{-4}
7.68×10^{-4}	5.99×10^{-4}
5.10×10^{-4}	7.20×10^{-4}
5.06×10^{-4}	7.44×10^{-4}
4.91×10^{-4}	7.44×10^{-4}
4.41×10^{-4}	7.70×10^{-4}
3.86×10^{-4}	8.11×10^{-4}
3.55×10^{-4}	8.29×10^{-4}

TABLE E-3

Preston Tube Data the Flat Plate

With A Porous Wall Cases

$x = 12.7$ cm

$D = 0.073$ cm

$\frac{\dot{m}_j}{\rho_\infty u_\infty (1)}$	$C_f = \frac{\tau}{1/2 \rho_e u_e^2}$
4.582×10^{-4}	11.23×10^{-4}
9.535×10^{-4}	8.65×10^{-4}
22.369×10^{-4}	8.70×10^{-4}
24.453×10^{-4}	8.56×10^{-4}
26.746×10^{-4}	8.30×10^{-4}
30.645×10^{-4}	8.15×10^{-4}

TABLE E-4

Preston Tube Data the Flat Plate

With A Porous Wall Cases

$x = 12.7$ cm

$D = 0.241$ cm

$\frac{\dot{m}_j}{\rho_\infty u_\infty (1)}$	$C_f = \frac{\tau}{1/2 \rho_e u_e^2}$
4.582×10^{-4}	9.44×10^{-4}
9.535×10^{-4}	6.72×10^{-4}
22.369×10^{-4}	6.80×10^{-4}
24.453×10^{-4}	6.73×10^{-4}
26.746×10^{-4}	6.48×10^{-4}
30.645×10^{-4}	6.23×10^{-4}

TABLE E-5

Preston Tube Data for Slot/Porous Wall

Combination Cases

x = 12.7 cm

(a) D = 0.073 cm

Portion	$\frac{\dot{m}_j}{\rho_\infty u_\infty (1)}$	$C_f = \frac{\tau}{1/2 \rho_e u_e^2}$
(1) Slot	6.275×10^{-4}	7.41×10^{-4}
(1) Porous	6.243×10^{-4}	7.41×10^{-4}
(2) Slot	7.994×10^{-4}	7.46×10^{-4}

(b) D = 0.241 cm

Portion	$\frac{\dot{m}_j}{\rho_\infty u_\infty (1)}$	$C_f = \frac{\tau}{1/2 \rho_e u_e^2}$
(1) Slot	6.275×10^{-4}	4.57×10^{-4}
(1) Porous	6.243×10^{-4}	4.57×10^{-4}
(2) Porous	4.040×10^{-4}	7.46×10^{-4}

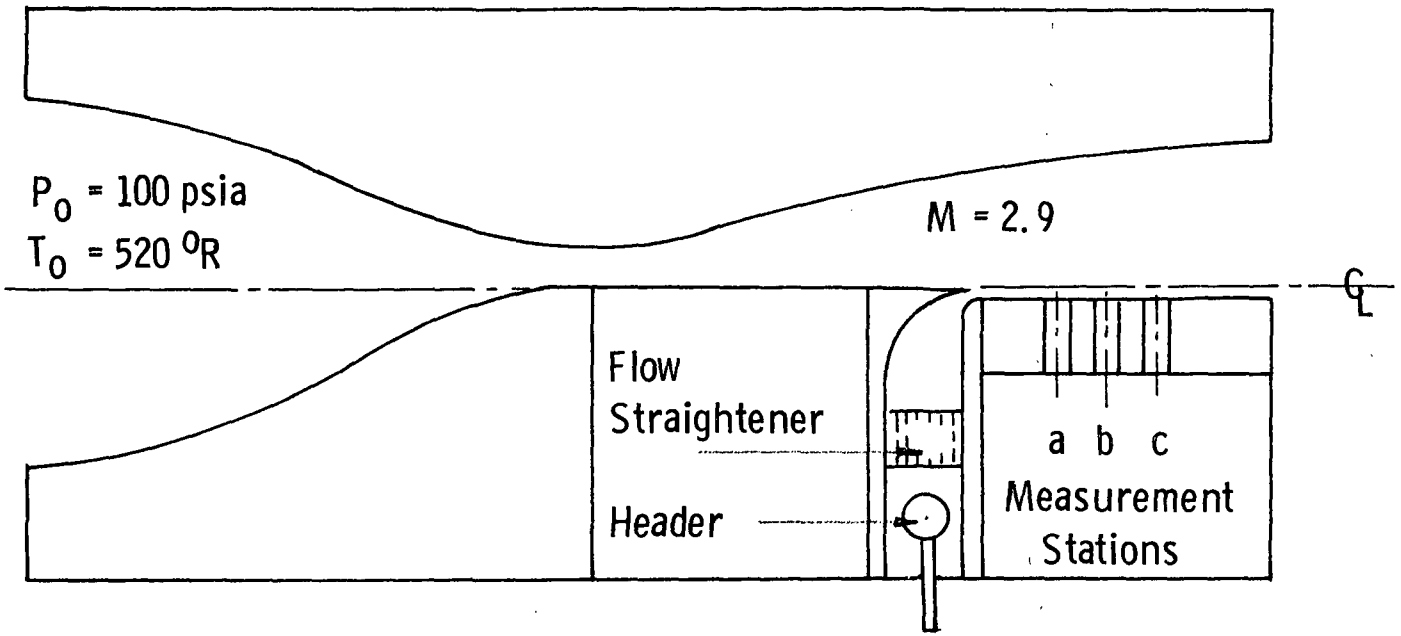

Fig. No. 1(a) - Model Configuration for Slot-Only Tests

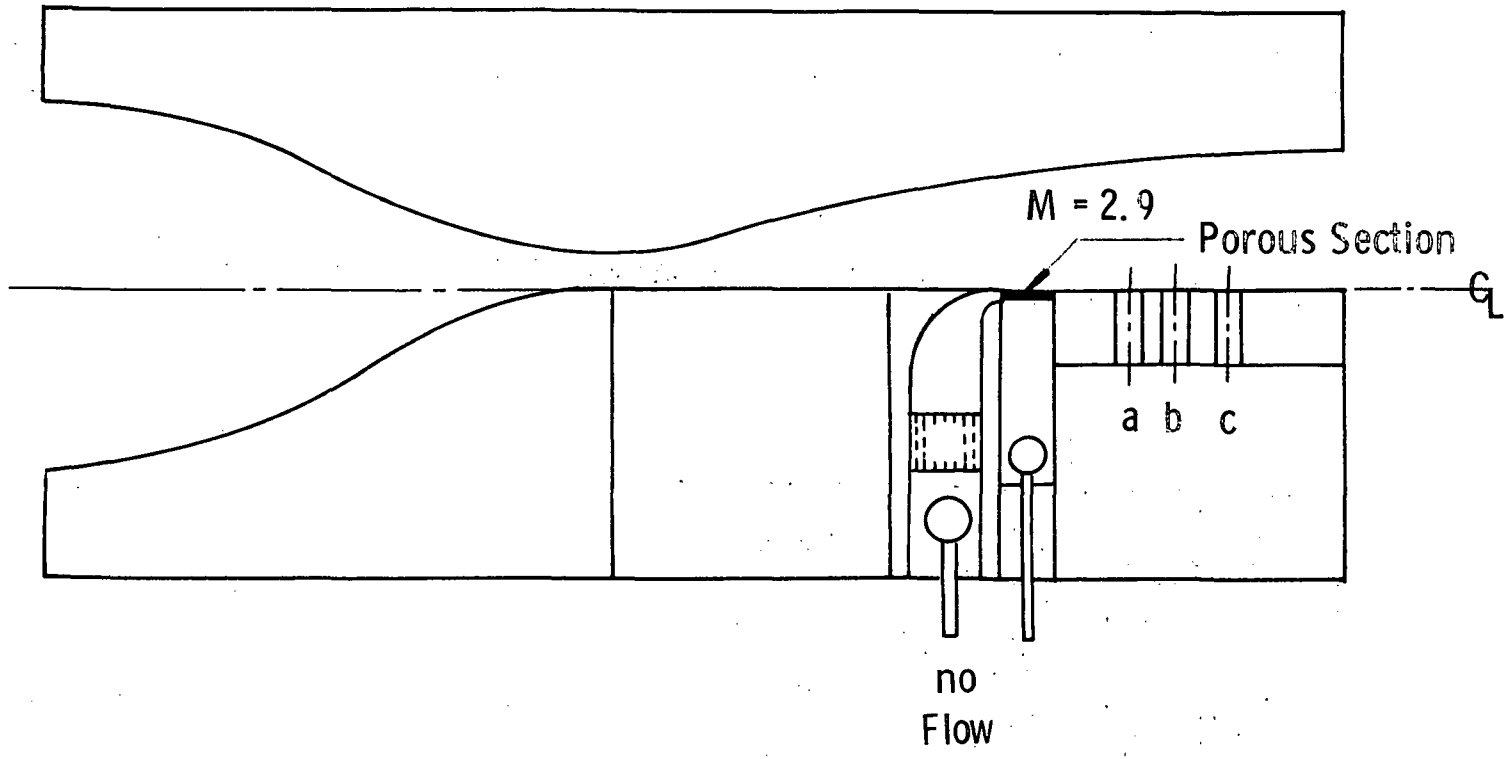

Fig. No. 1(b) - Model Configuration for Porous Wall Section Tests

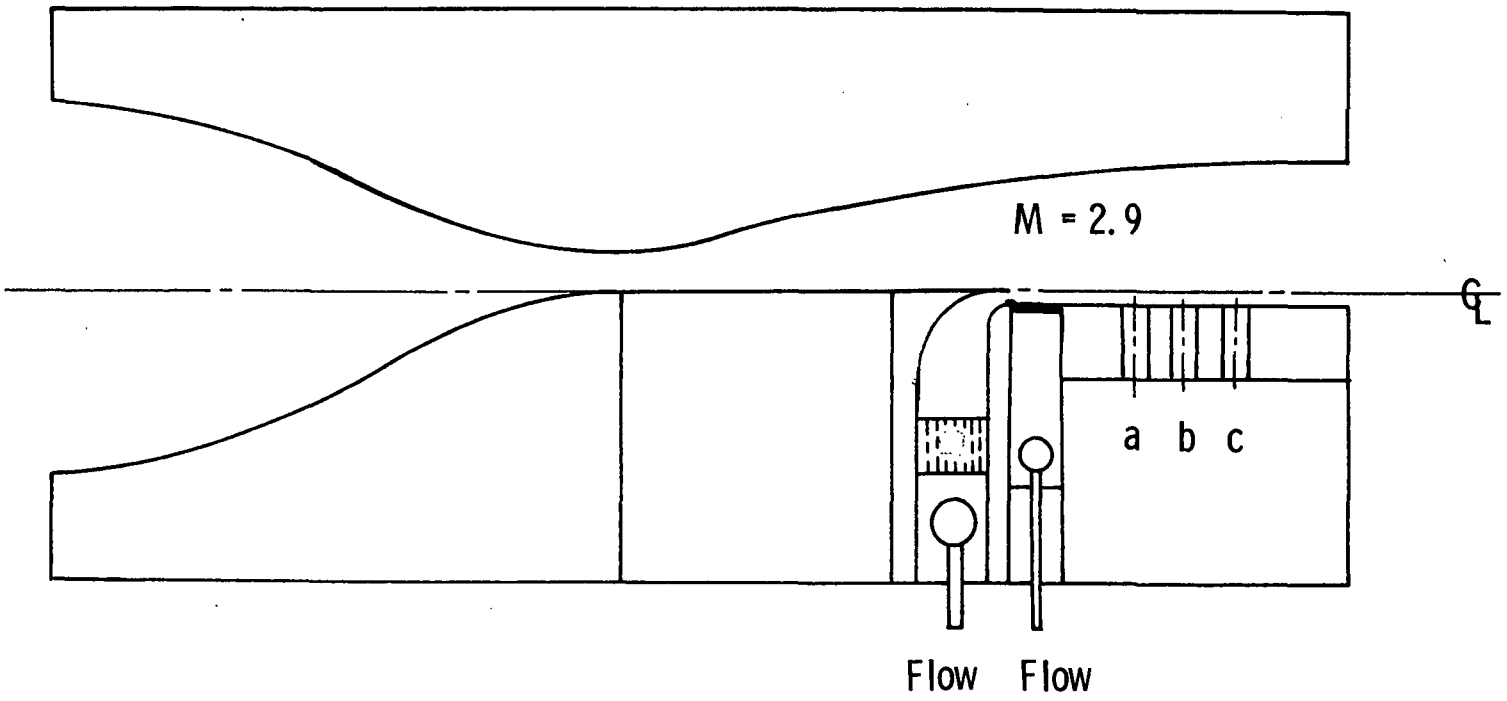

Fig. No. 1(c) - Model Configuration for Slot/Porous Section Combination Tests

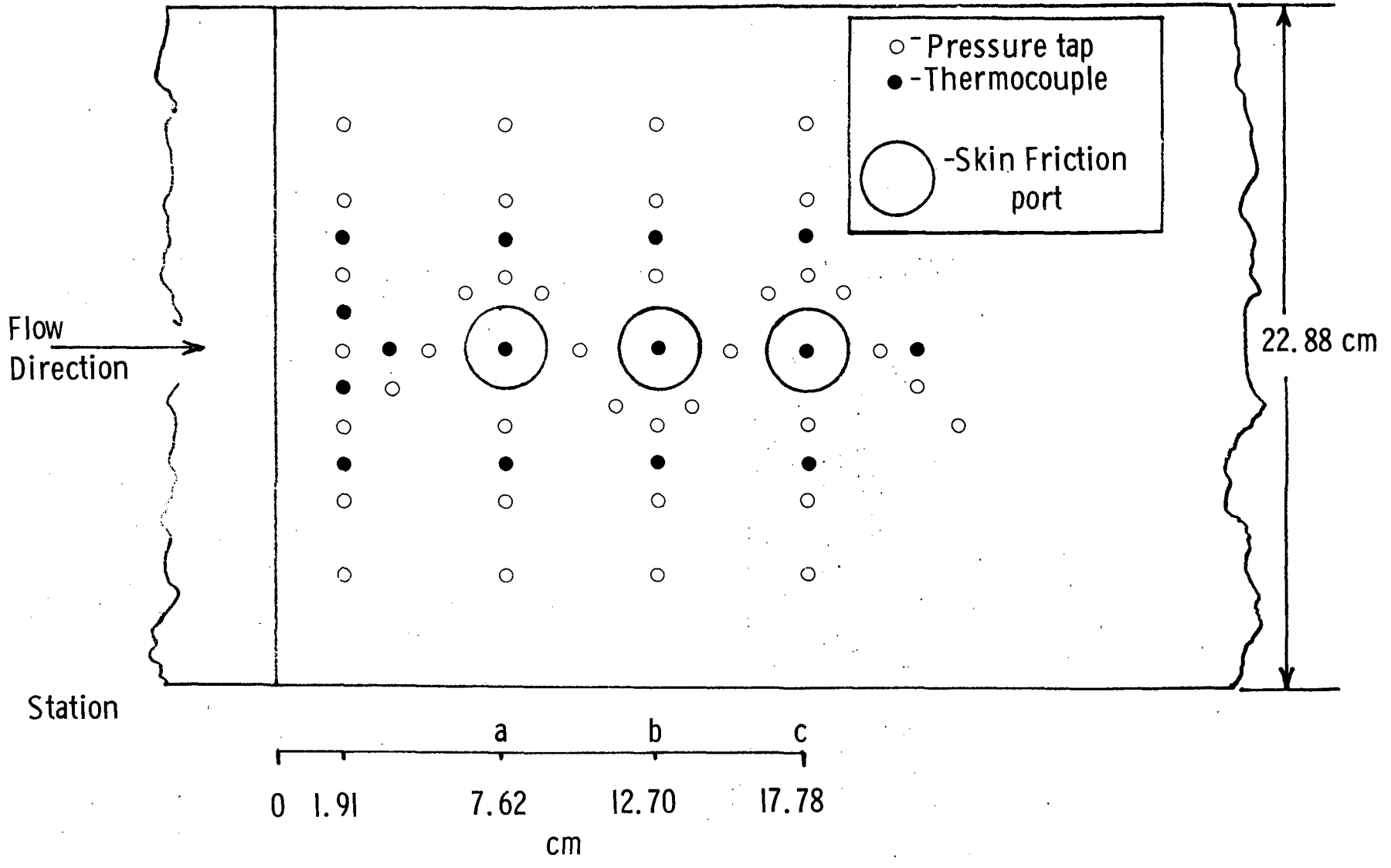

Fig. No. 2 Instrumented wall section

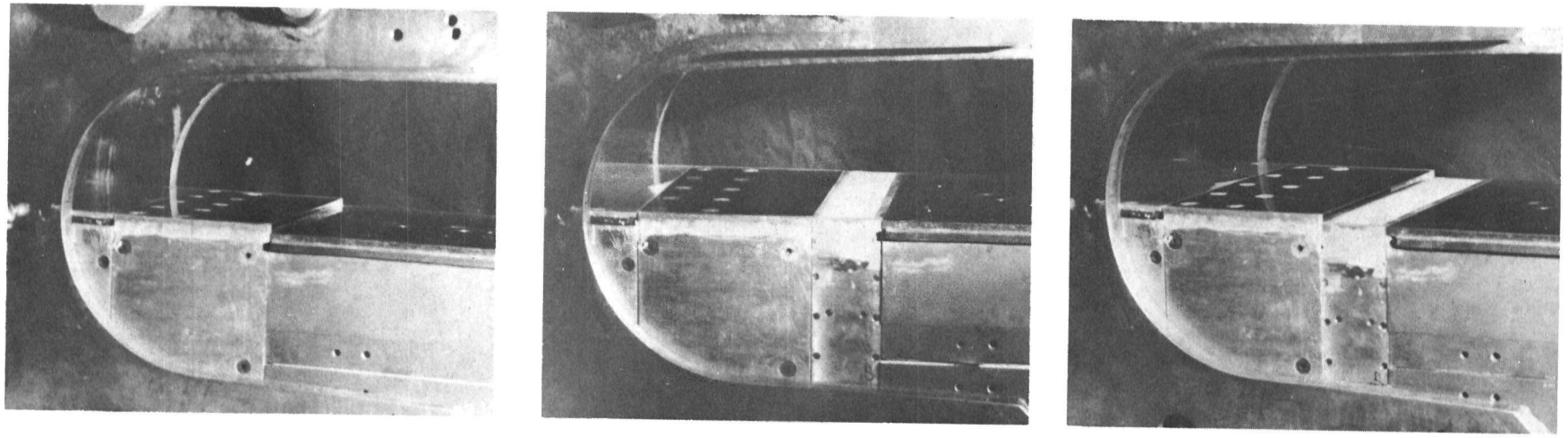

(a) Slot only

(b) Porous wall

(c) Slot / Porous wall combination

Fig. No. 3 Photographs of the injection models

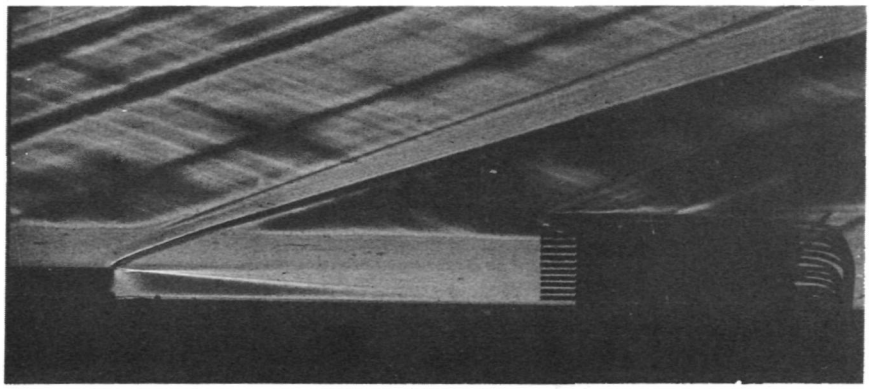

(a) Slot only

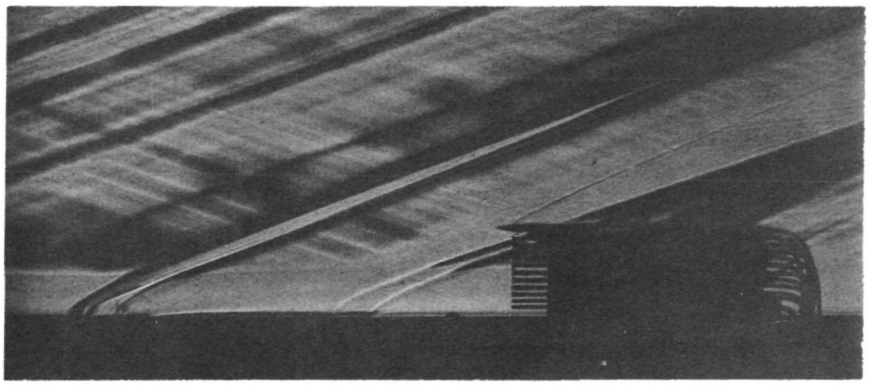

(b) Porous wall

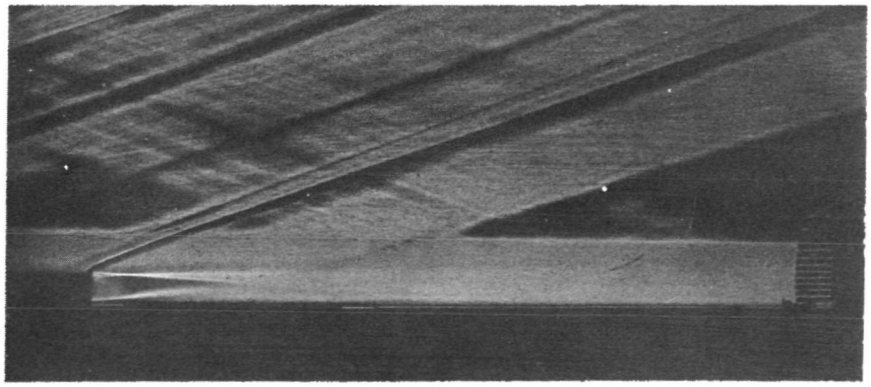

(c) Slot / Porous wall combination

Fig. No. 4 Schlieren photographs

	$\left[\frac{\dot{m}_j}{\rho_\infty u_\infty (1)}\right]$
POSITION 1	6.94×10^{-4}
POSITION 2	7.36×10^{-4}
POSITION 3	7.26×10^{-4}

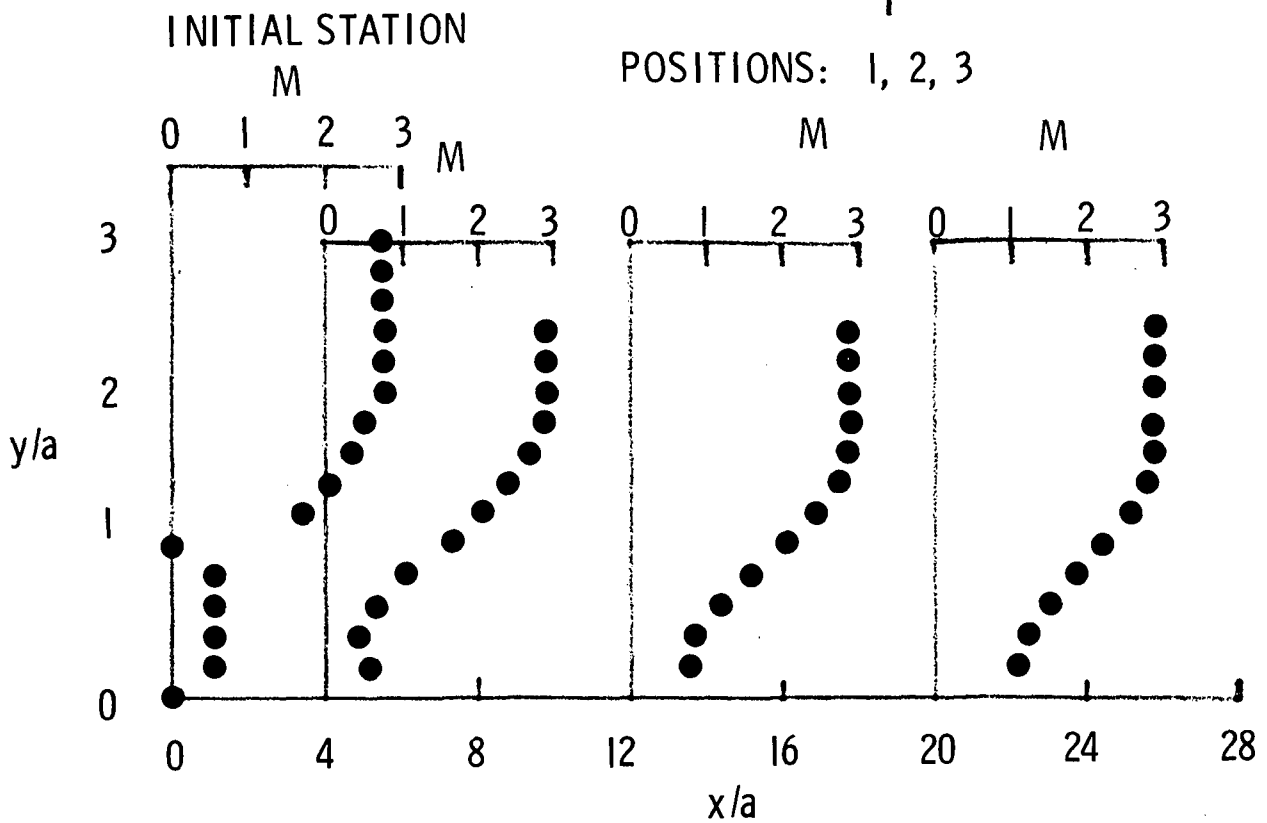

(a) Slot only

Fig. No. 5 Typical Mach number profiles

□	$\left[\frac{\dot{m}_j}{\rho_\infty u_\infty (l)}\right]$
POSITION 1	1.072×10^{-3}
POSITION 2	1.034×10^{-3}
POSITION 3	--

○	$\left[\frac{\dot{m}_j}{\rho_\infty u_\infty (l)}\right]$
POSITION 1	5.76×10^{-4}
POSITION 2	--
POSITION 3	5.51×10^{-4}

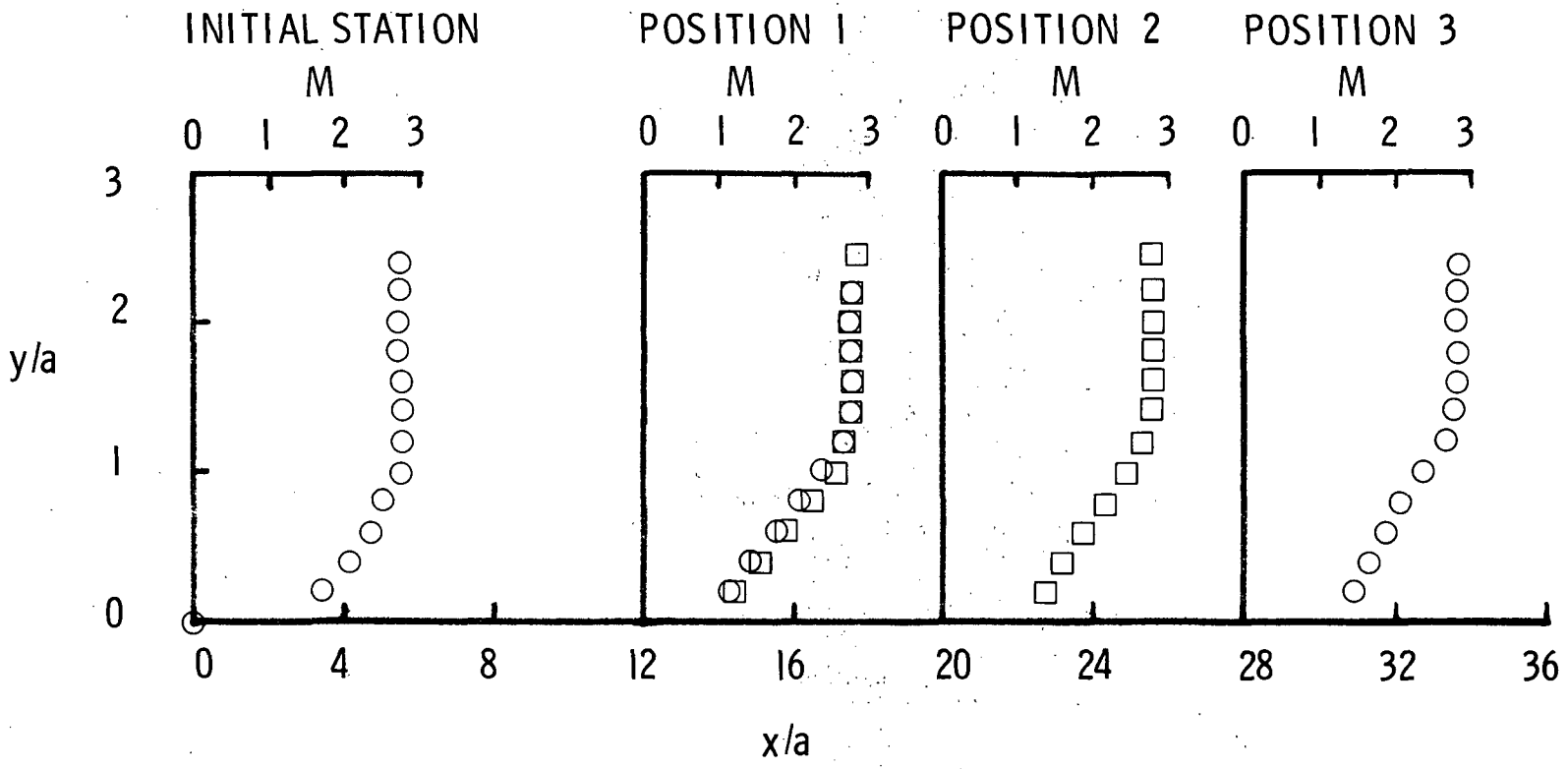

5 (b) Porous wall

$$\left[\frac{\dot{m}_j}{\rho_\infty u_\infty(1)}\right] = 1.324 \times 10^{-3}$$

○ 70% Slot/ 30% Porous

□ 47.1% Slot/ 52.9% Porous

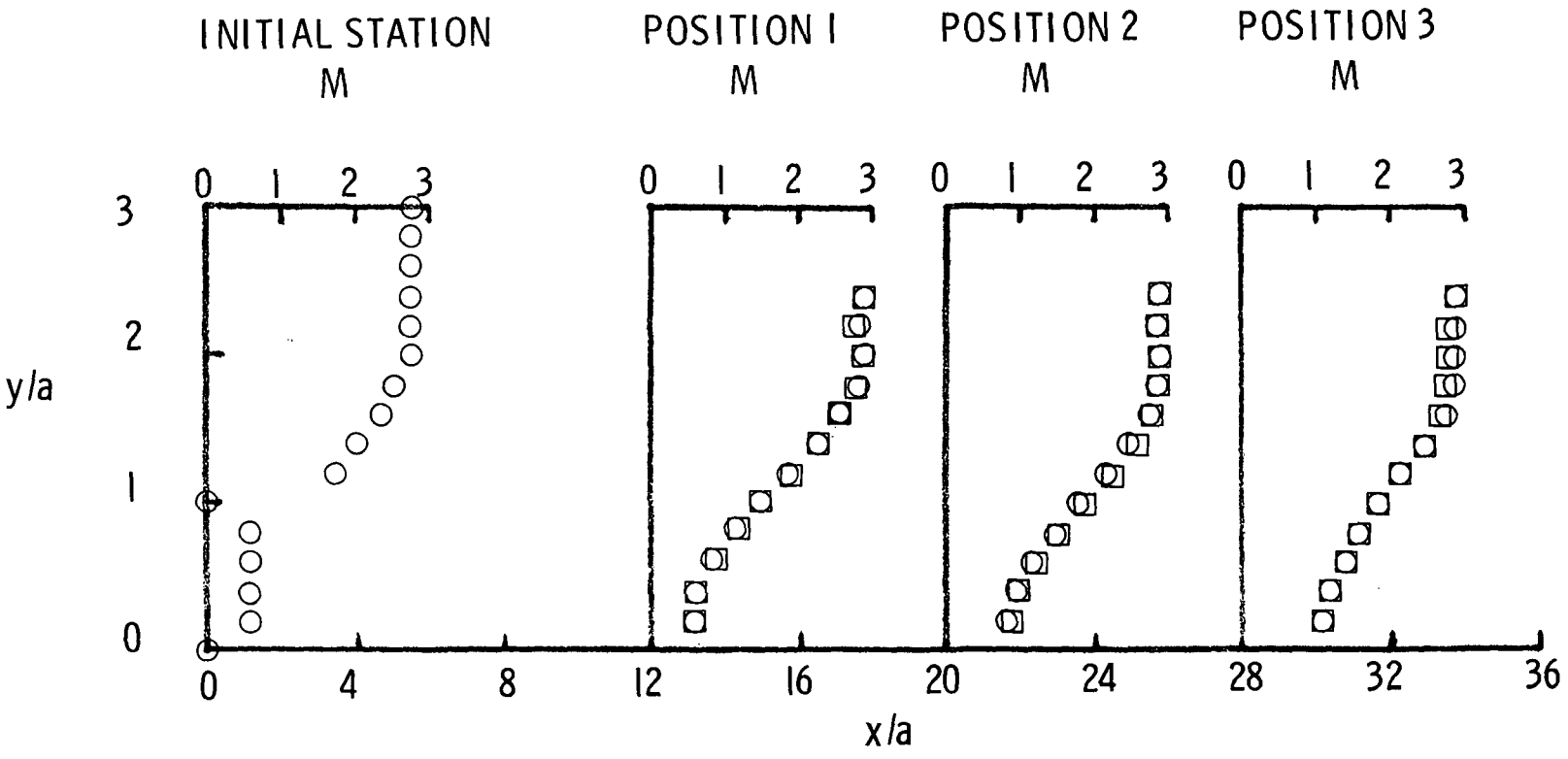

5 (c) Slot / Porous wall combination

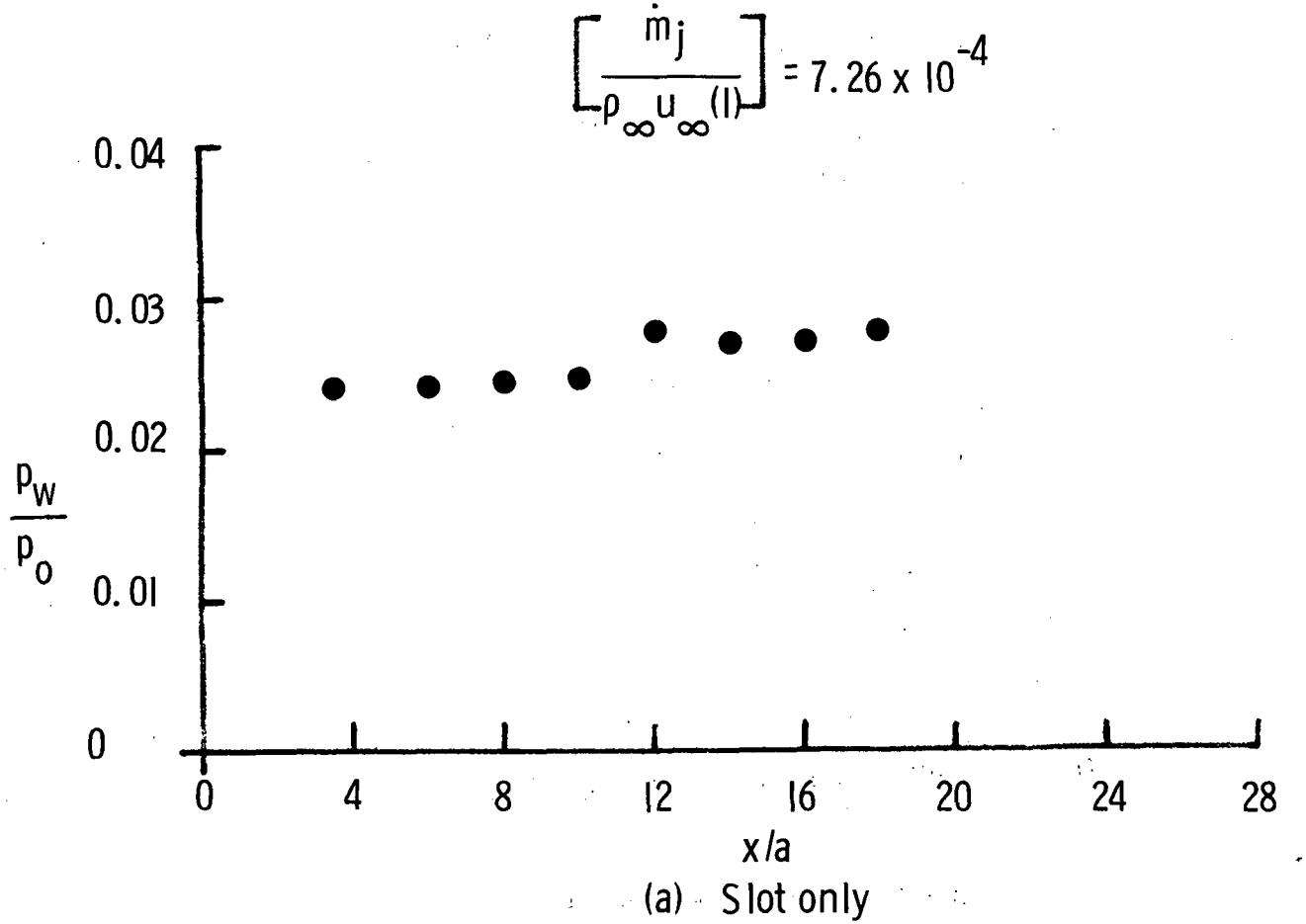

(a) Slot only

Fig. No. 6 Wall pressure distributions

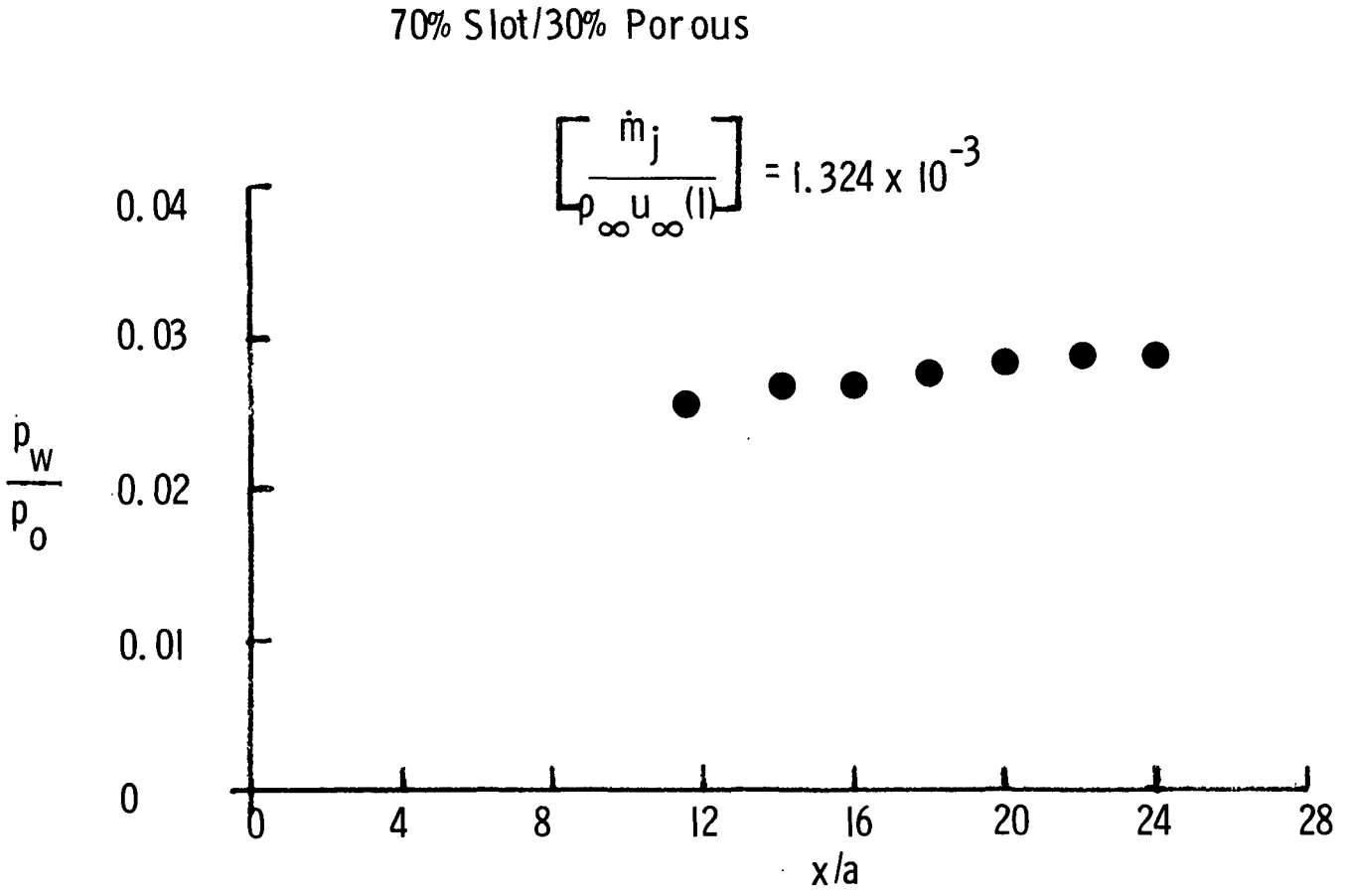

6 (b) Slot / Porous wall combination

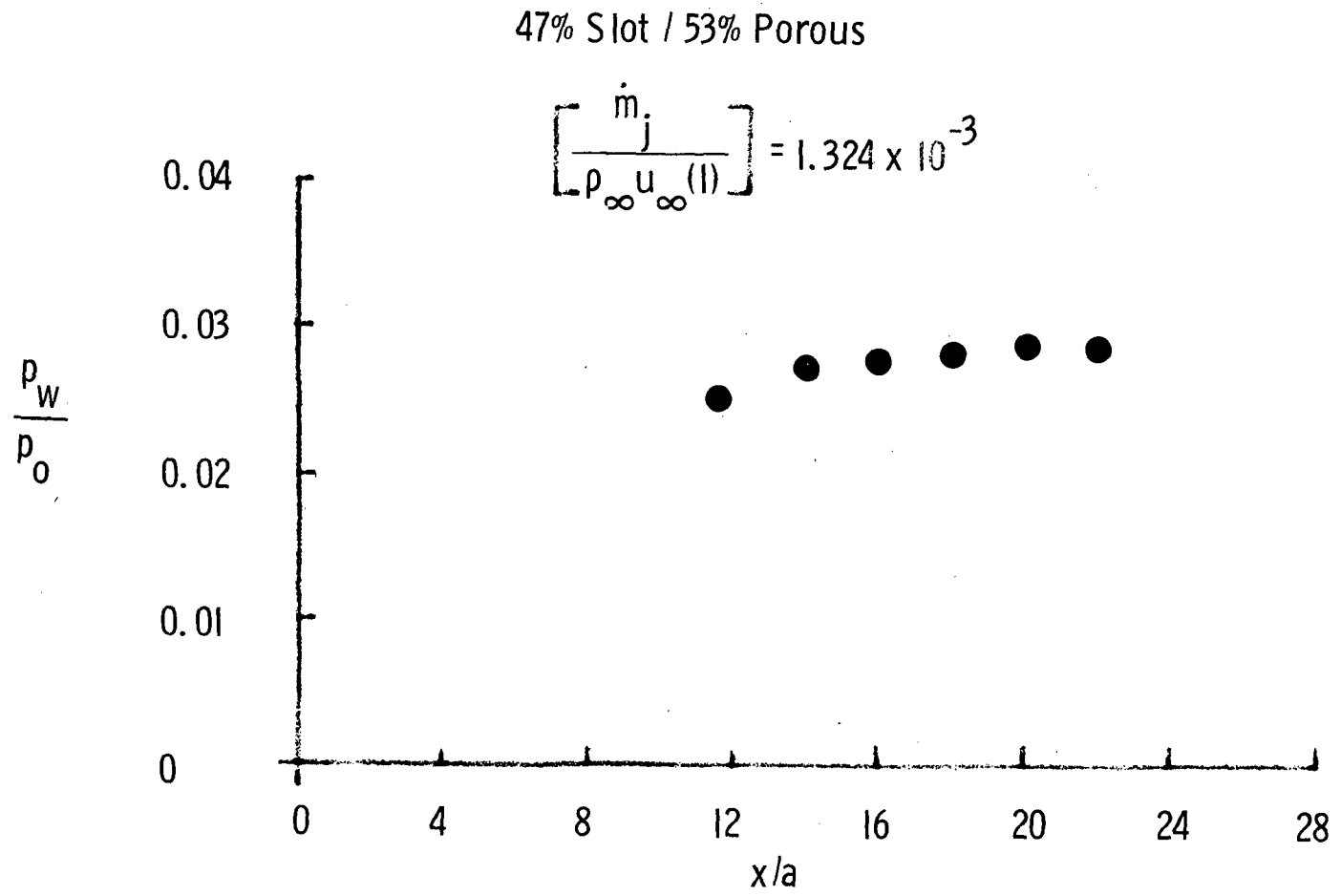

6 (c) Slot/Porous wall combination

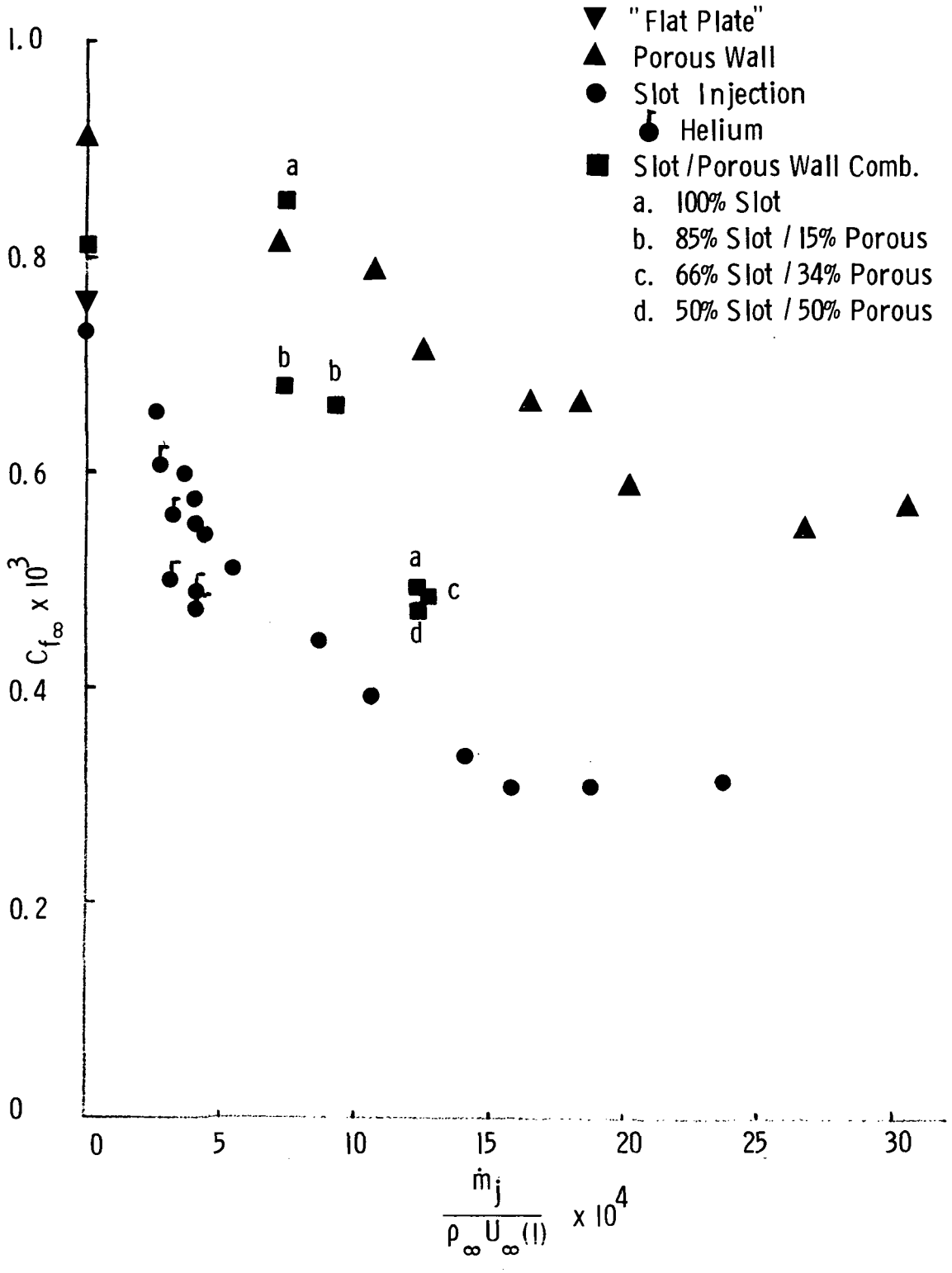

Fig. No. 7 Skin friction balance data

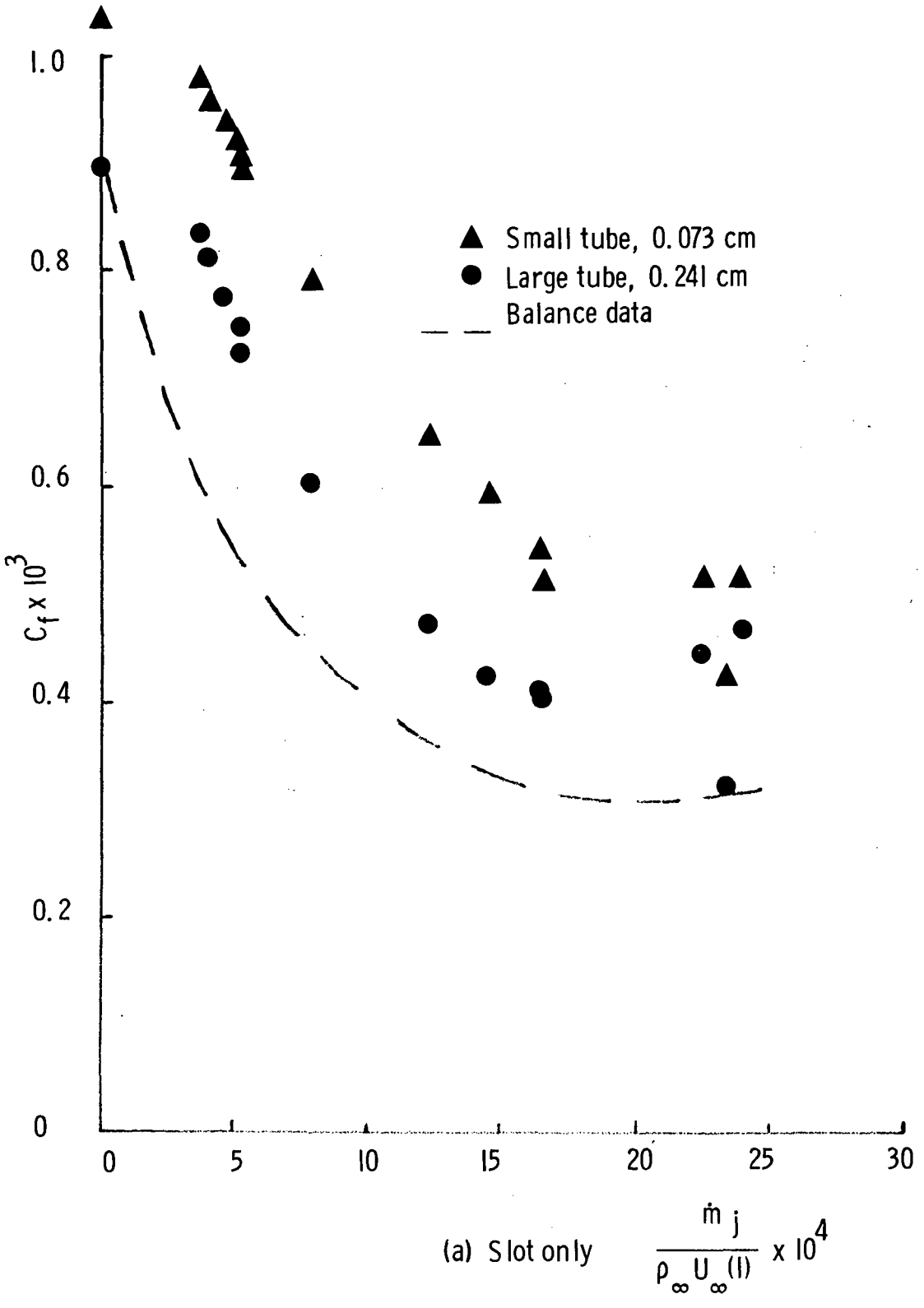

Fig. No. 8 Preston tube data

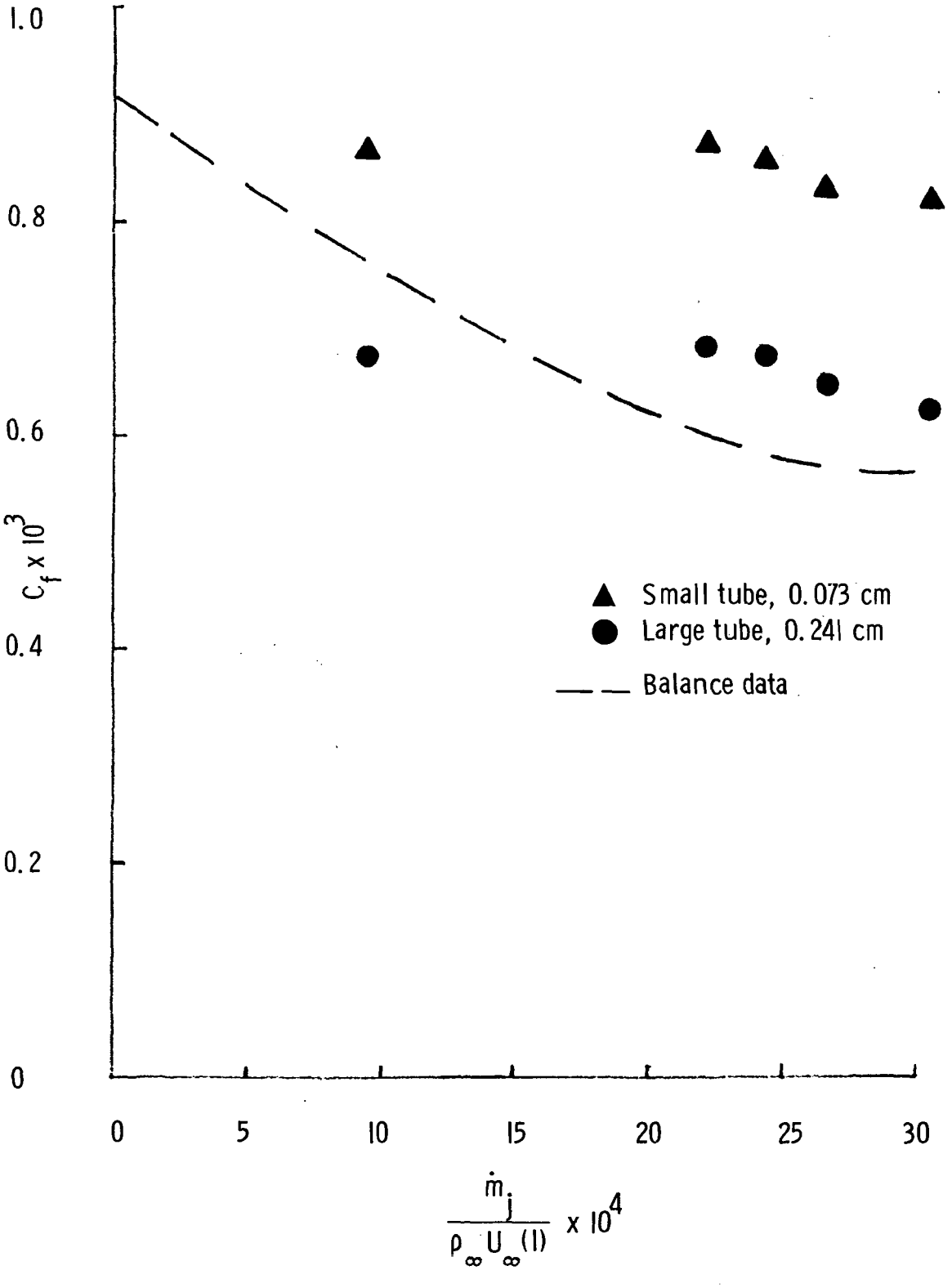

(b) Porous wall

NATIONAL AERONAUTICS AND SPACE ADMINISTRATION
WASHINGTON, D.C. 20546

OFFICIAL BUSINESS
PENALTY FOR PRIVATE USE $300

SPECIAL FOURTH-CLASS RATE BOOK

POSTAGE AND FEES PAID
NATIONAL AERONAUTICS AND SPACE ADMINISTRATION
451

U.S.MAIL

POSTMASTER: If Undeliverable (Section 158 Postal Manual) Do Not Return

"The aeronautical and space activities of the United States shall be conducted so as to contribute . . . to the expansion of human knowledge of phenomena in the atmosphere and space. The Administration shall provide for the widest practicable and appropriate dissemination of information concerning its activities and the results thereof."

—NATIONAL AERONAUTICS AND SPACE ACT OF 1958

NASA SCIENTIFIC AND TECHNICAL PUBLICATIONS

TECHNICAL REPORTS: Scientific and technical information considered important, complete, and a lasting contribution to existing knowledge.

TECHNICAL NOTES: Information less broad in scope but nevertheless of importance as a contribution to existing knowledge.

TECHNICAL MEMORANDUMS: Information receiving limited distribution because of preliminary data, security classification, or other reasons. Also includes conference proceedings with either limited or unlimited distribution.

CONTRACTOR REPORTS: Scientific and technical information generated under a NASA contract or grant and considered an important contribution to existing knowledge.

TECHNICAL TRANSLATIONS: Information published in a foreign language considered to merit NASA distribution in English.

SPECIAL PUBLICATIONS: Information derived from or of value to NASA activities. Publications include final reports of major projects, monographs, data compilations, handbooks, sourcebooks, and special bibliographies.

TECHNOLOGY UTILIZATION PUBLICATIONS: Information on technology used by NASA that may be of particular interest in commercial and other non-aerospace applications. Publications include Tech Briefs, Technology Utilization Reports and Technology Surveys.

Details on the availability of these publications may be obtained from:

SCIENTIFIC AND TECHNICAL INFORMATION OFFICE

NATIONAL AERONAUTICS AND SPACE ADMINISTRATION

Washington, D.C. 20546